

Impact of modelling galaxy redshift uncertainties on the gravitational-wave dark standard siren measurement of the Hubble constant

Cezary Turcki,^{1*} Maciej Bilicki,² Gergely Dályi,¹ Rachel Gray,^{3,4} and Archisman Ghosh¹

¹*Department of Physics & Astronomy, Ghent University, Proeftuinstraat 86, 9000 Ghent, Belgium*

²*Center for Theoretical Physics, Polish Academy of Sciences, al. Lotników 32/46, 02-668 Warsaw, Poland*

³*Department of Physics & Astronomy, Queen Mary University of London, Mile End Road, London, E1 4NS, United Kingdom*

⁴*SUPA, University of Glasgow, Glasgow, G12 8QQ, United Kingdom*

Accepted XXX. Received YYY; in original form ZZZ

ABSTRACT

Gravitational wave science is a new and rapidly expanding field of observational astronomy. Multimessenger observations of the binary neutron star merger GW170817 have provided some iconic results including the first gravitational-wave standard-siren measurement of the Hubble constant, opening up a new way to probe cosmology. The majority of the compact binary sources observed in gravitational waves are however without bright electromagnetic counterparts. In these cases, one can fall back on the “dark standard siren” approach to include information statistically from potential host galaxies. For such a measurement, we need to be cautious about all possible sources of systematic errors. In this paper, we begin to study the possible errors coming from the galaxy catalogue sector, and in particular, look into the effect of galaxy redshift uncertainties for the cases where these are photometry-based. We recalculate the dark standard siren Hubble constant using the latest GWTC-3 events and associated galaxy catalogues, with different galaxy redshift uncertainty models, namely, the standard Gaussian, a modified Lorentzian, and no uncertainty at all. We find that not using redshift uncertainties at all can lead to a potential bias comparable with other potential systematic effects previously considered for the GWTC-3 H_0 measurement (however still small compared to the overall statistical error in this measurement). The difference between different uncertainty models leads to small differences in the results for the current data; their impact is much smaller than the current statistical errors and other potential sources of systematic errors which have been considered in previous robustness studies.

Key words: gravitational waves — cosmological parameters — galaxies: distances and redshifts

1 INTRODUCTION

The discovery of gravitational waves (GWs) has opened a new window to astronomical observations (Abbott et al. 2016). The latest Third Gravitational-Wave Transient Catalogue (GWTC-3) of mergers of black holes (BHs) and neutron stars (NSs) contains 90 events observed by the LIGO-Virgo-KAGRA detector network (Abbott et al. 2021a). Among the many scientific results obtained using these observations is a novel GW measurement of the Hubble constant H_0 (Abbott et al. 2021b). Future observing runs with increasing detector sensitivities are expected to detect many more such compact binaries. The large number of events expected in the coming years offer the potential to precisely probe the cosmological parameters governing the expansion of the universe.

The possibility of using GWs to determine the Hubble constant H_0 was proposed by Schutz (1986), where he pointed out that the luminosity distance of compact binary coalescences can be measured directly from the observed GW data. These sources are thus self-calibrated distance indicators, or ‘standard sirens’. If a successful electromagnetic (EM) follow-up campaign can identify the host

galaxy of the event, H_0 can be in principle determined using the distance and the host galaxy’s redshift (Schutz 1986; Holz & Hughes 2005; MacLeod & Hogan 2008; Nissanke et al. 2010; Abbott et al. 2017). Furthermore, even if an EM counterpart cannot be identified, a statistical analysis using galaxy data from the localization region can be a viable alternative, given a large enough number of observations (Schutz 1986; Del Pozzo 2012; Chen et al. 2018; Fishbach et al. 2019a; Soares-Santos et al. 2019; Gray et al. 2020; Abbott et al. 2021d, 2020; Palmese et al. 2020; Finke et al. 2021; Abbott et al. 2021b; Palmese et al. 2023). These events, for which no counterpart is observed, are now called ‘dark sirens’. Over the preceding years, it has become clear that the source-frame mass distribution of the compact binaries as well as the redshift prior from a galaxy catalogue play a role in a dark standard siren measurement (Taylor et al. 2012; Farr et al. 2019; Mastroianni et al. 2021).

Inferring H_0 from GW observations may help to resolve the Hubble tension (see e.g. Dainotti et al. 2021, 2022) – the statistically significant difference between H_0 values obtained by methods based on early-Universe measurements, using the cosmic microwave background radiation ($H_0 = 67.36 \pm 0.54 \text{ km s}^{-1} \text{ Mpc}^{-1}$; Aghanim et al. 2020) and those obtained from late-Universe measurements, relying on the cosmic distance ladder ($H_0 = 73.04 \pm 1.04 \text{ km s}^{-1} \text{ Mpc}^{-1}$;

* E-mail: cezary.turski@ugent.be (CT)

Riess et al. 2022). The current best GW measurement of H_0 using 47 events from GWTC-3 yields $H_0 = 68^{+12}_{-8}$ km s⁻¹Mpc⁻¹ (Abbott et al. 2021b). Given the large uncertainty, this is in agreement with both early-type and late-type methods. In the coming years, an increase in precision of the instruments leading to a higher number of events, as well as improved methodology, will lead to a more precise measurement. As we move towards that goal, we need to carefully investigate and mitigate the various systematic effects, both on the GW and on the EM side, which enter the data and the associated assumptions.

It is worth mentioning that standard sirens potentially probe not only the local expansion rate of the universe but also the non-linear Hubble parameter $h(z)$, potentially constraining other parameters of the Λ -CDM cosmological model such as the matter density fraction Ω_m or the dark energy equation-of-state parameter w_0 . In this paper, we only consider the current set of detections. With a handful of nearby observations that we have at the moment, constraints on the latter parameters are not very meaningful (see, e.g., Figure 4 of Abbott et al. 2021b).

It has already been demonstrated in Abbott et al. (2021b) that the unknown population distribution of GW sources is the leading source of systematic uncertainty, at least for the GWTC-3 measurement of H_0 with the galaxy catalogue method, where the uncertainty in the population has not yet been marginalised over. This is largely because of the relatively low level of completeness of the associated galaxy catalogues – we are currently dominated by the so-called out-of-catalogue part in the result. The situation may change once we are able to use deeper surveys and the in-catalogue part becomes more important. Potential uncertainties coming from the EM sector have not been extensively studied for dark standard siren measurements, an exception being the work of Palmese et al. (2020) where two approaches of modelling redshift uncertainties were discussed. It is worth noting that there are several studies on potential systematic effects from peculiar velocities of galaxies (e.g., Howlett & Davis 2020; Mukherjee et al. 2021; Nicolaou et al. 2020). However these effects are relevant particularly for a H_0 measurement coming from a handful of nearby events (i.e., bright standard sirens). Peculiar velocities are relatively small for bright standard sirens which are typically more distant events, and they are further expected to average or cancel out over a large number of observations required for a reasonable H_0 measurement. For dark standard sirens, redshift measurement uncertainties are thus expected to be the significant source of error in the EM sector.

In current dark siren measurements of H_0 , the galaxy catalogues used include only a small fraction of exact spectroscopic redshifts. Most of the redshifts in such wide-angle datasets are instead estimated from galaxy multi-band photometry (photometric redshifts, photo-zs). Despite such extensive spectroscopic surveys as DESI (DESI Collaboration et al. 2016), 4MOST (de Jong et al. 2019) or Euclid (Laureijs et al. 2011), this situation is unlikely to change in the coming years. Photometric redshifts bear considerable uncertainties (typically 10% or more) and this can influence related analyses. In this paper, we investigate the impact of redshift uncertainty models on the dark standard siren H_0 measurement. We first study redshift uncertainty models which capture more features than a simple Gaussian profile. In particular, we model the uncertainty in the redshift of a potential host galaxy as a modified Lorentzian distribution and fit its parameters to data from the 2 Micron All-Sky Survey Photometric Redshift Catalogue (2MPZ, Bilicki et al. 2014) and the WISExSCOS Photometric Redshift Catalogue (WISC, Bilicki et al. 2016). Subsequently, we modify the standard gwcsmo pipeline used for H_0 inference (Gray et al. 2020, 2022) to include different red-

shift uncertainty models other than the previously-used simplistic Gaussian model. Finally, in order to estimate the impact of redshift uncertainties, we compute H_0 using the 47 events from GWTC-3 used in Abbott et al. (2021b) and the different uncertainty models for each of the two catalogues above.

The rest of this paper is organised as follows. We describe our choice of galaxy catalogues in Section 2 and go over our modelling of redshift uncertainties in Section 3. We review our H_0 inference method and present the settings and the associated GW data in Section 4. We describe and discuss our results in Section 5. In the same section, we also include a brief discussion of how redshift uncertainties can impact the in-catalogue and out-of-catalogue components of a H_0 inference method. We conclude and mention a few items for follow-up work in Section 6. There are two appendices which provide additional details on some specific aspects of Section 3 and Section 5 respectively.

2 ELECTROMAGNETIC DATA

The GLADE+ galaxy catalogue (Dályá et al. 2022) was used to obtain electromagnetic data for the most recent GW H_0 inference by the LVK collaboration. GLADE+ is an expanded version of the GLADE sample (Dályá et al. 2018), which had previously been used in several cosmological studies (see e.g. Fishbach et al. 2019b; Abbott et al. 2020, 2021d). As GLADE+ is a composite galaxy catalogue created by combining data from six different astronomical databases (White et al. 2011; Bilicki et al. 2014; Skrutskie et al. 2006; Makarov et al. 2014; Bilicki et al. 2016; Lyke et al. 2020) with different properties, such a sample could not be easily applied within our methodology, which requires a particular photo-z error model for a given galaxy dataset (see Section 3). Hence, here we use two of the major constituent catalogues of GLADE+, 2MPZ and WISC. These two catalogues offer the main advantages of covering very large areas of the sky and having well-controlled selections and photo-z performance; this is especially the case for 2MPZ. They also have a number of drawbacks, though, such as optical photometry from the photographic era, very limited depth (especially in 2MPZ), and occasionally complicated source selection, joining the optical, near-, and mid-infrared. These issues are now very much resolved in new datasets such as Pan-STARRS (Chambers et al. 2016) or the DESI Legacy Imaging Survey (Dey et al. 2019) and we plan to use such updated samples for related studies in the future. For this work, however, the 2MPZ and WISC catalogues will suffice as a good test-bed for leading order effects of photo-z uncertainties on H_0 derivation from GW events within the statistical method.

Both 2MPZ and WISC are multi-band photometric catalogues that were created by combining all-sky legacy optical photometry obtained from digitised photographic plates (SuperCOSMOS; Hambly et al. 2001; Peacock et al. 2016) with infrared datasets. In the 2MPZ case, these latter were the Two Micron All Sky Survey Extended Source Catalogue (2MASS XSC; Skrutskie et al. 2006; Jarrett et al. 2000) and the Wide-field Infrared Survey Explorer (WISE; Wright et al. 2010) from its "All-Sky" data release (Cutri et al. 2012). This provided nearly 1 million galaxies over most of the sky with 9-band photometric coverage, including photographic B_J , R , and I , near-IR J , H , and K_s , and mid-IR $W1$ and $W2$. In WISC, 2MASS was no longer used, while WISE data originated from the subsequent "AllWISE" catalogue (Cutri et al. 2021). The resulting cross-match includes nearly 20 million galaxies, reliably covering about 70% of the sky in four bands, $B_J R W1 W2$. In the 2MPZ case, its depth is driven by the shallowest of the 3 input datasets, 2MASS XSC, and it

is effectively a K_s -band-selected sample, flux-limited to $K_s < 13.9$ mag (Vega). Its median redshift is $z = 0.07$ and it has practically no galaxies beyond $z \sim 0.25$. WISC has a slightly more complicated selection, being flux-limited in three bands jointly: $B_J < 21$, $R < 19.5$ (both AB-like), and $W1 < 17$ (Vega). It is about 3 times deeper than 2MPZ, with $z_{\text{med}} \simeq 0.2$ and reaching up to $z \sim 0.45$.

The multi-band photometry of 2MPZ and WISC was further employed to obtain photo- z s for all the included galaxies. This was done via supervised machine-learning (ML) methodology, where a model is "trained" on ground-truth data to deliver predictions for a given quantity in an output sample. In this case, the mapping of interest is between photometry and redshift, and the ML method used was artificial neural networks (ANN) as implemented in the public "ANNz" package (Collister & Lahav 2004). The training sets include galaxies that overlap between the photometric datasets and the external spectroscopic redshift (spec- z) samples; the latter redshift measurements are typically accurate enough to assume that they have no errors that could influence the ML training. The spec- z data used for the training sets was chosen in a way to best match the depth of the photometric samples. For 2MPZ, these were mostly based on the 2MASS Redshift Survey (Huchra et al. 2012), the 6dF Galaxy Survey (Jones et al. 2009), the 2dF Galaxy Redshift Survey (Colless et al. 2001) and the Sloan Digital Sky Survey Data Release 9 (Ahn et al. 2012). In WISC, the photo- z training sample was derived from a cross-match with the Galaxy And Mass Assembly (Driver et al. 2009) from its "GAMA-II" catalogues (Liske et al. 2015). Additionally, SDSS DR12 (Alam et al. 2015) was used to calibrate the purification of the WISC dataset from stars and quasars.

3 MODELING THE REDSHIFT UNCERTAINTIES

Photometric redshifts often have large uncertainties and non-trivial error profiles. Using an inaccurate uncertainty profile may lead to a bias in H_0 Palmese et al. (2020), so reliable photo- z error estimates are needed. In an ideal scenario, one could use uncertainty quantification provided for instance by the photo- z algorithm, for each of the considered EM sources. This was for instance applied in Palmese et al. (2020) for the Dark Energy Survey (DES) galaxies and the associated DNF photo- z estimation algorithm. There the authors compare the case when individual photo- z probability density functions are used, to the case of Gaussian approximation. Out of the two events they consider, only one leads to a notable difference in the H_0 posterior. Hence, it still remains to be seen how important this approach would be for a considerably larger dataset. Unfortunately, most of the photo- z methodologies, especially those ML-based, do not reliably deliver such information for the individual objects. This is not different in the case of ANNz-derived photo- z s in the 2MPZ and WISC catalogues which we consider. What can be however done, is to calibrate the photo- z uncertainties *a posteriori*, by comparing the photo- z s with overlapping spec- z samples and analyzing the redshift residuals, $\Delta z \equiv z_{\text{photo}} - z_{\text{spec}}$ (often additional rescaled by $1 + z$). In practice, such a model cannot usually be obtained for each individual source separately. It is however possible to build more general photo- z error models as a function of redshift, magnitude or possibly also galaxy color. In this work, we look at this first option and construct photo- z error models for 2MPZ and WISC as a function of photometric redshift, which is the most relevant as an 'observable' (unlike spec- z , which is not available for most galaxies in a photo- z dataset). These photo- z error models provide the posterior distribution on the true redshift of each galaxy given the measured z_{photo} , $p(z|z_{\text{photo}})$.

The simplest photo- z error model is a Gaussian, with some mean

residual μ and scatter σ . It is however well known from the literature that even 'well-behaved' photo- z s (i.e. those for which errors are symmetric and centered at 0), usually have non-Gaussian tails. For instance, for the 2MPZ case, a better fit is obtained if a 'modified Lorentzian' is used (Bilicki et al. 2014). This distribution is given by

$$f(\Delta z) = A \left(1 + \frac{\Delta z^2}{2as^2} \right)^{-a} \quad (1)$$

where Δz is a difference between the photometric and spectroscopic redshift, A is a normalization factor, while a and s are free parameters that need to be inferred for the galaxy catalogue. Note that this is valid only when $a > 0.5$. The same model, albeit with different parameters than for 2MPZ, was also used for modelling the WISC photo- z uncertainties in Peacock & Bilicki (2018). The difference between Gaussian and modified Lorentzian uncertainty model is shown in Figure 1. In such a formulation, the average photo- z errors are assumed to be 0, which for 2MPZ and WISC is a sufficiently good approximation in the sense that the mean bias is much smaller than the scatter. We note however that the model could be generalised for non-zero average bias (e.g. Hang et al. 2021). Finally, other analytical formulations could be used to recover the non-Gaussian features, such as for instance the Student- t distribution (e.g. Vakili et al. 2020) or other empirically-driven fits (Balaguera-Antolínez et al. 2018).

As mentioned above, we will be modelling the photo- z uncertainties as functions of the "observed" photo- z itself. This will be done both for the simpler Gaussian case, where we will fit for both μ and σ (that is, our Gaussian models do not have to be centred on 0), and for the modified Lorentzian in the unbiased case (i.e. with free parameters a and s). In the most general case, all these parameters can be some general functions of photo- z , although we will limit ourselves to their linear evolution with z_{photo} . For that, we use spectroscopic calibration samples, thanks to which we can calculate redshift residuals Δz for the full range of z_{photo} of a given dataset. For the methodology to work properly, these calibration samples should be representative for the whole photometric dataset in question. This would ideally mean a random subsample of the entire catalogue, which is hardly ever available. The second-best scenario, that our calibration samples meet, is to use spec- z data from a flux-limited sample deeper than the calibrated photo- z catalogue. For 2MPZ, we employ all the spec- z samples overlapping with it, mentioned in the previous Section, the most useful of them being SDSS, which is deeper than 2MASS XSC. For WISC, such a calibration sample is provided by GAMA, which in its equatorial fields is a very complete, flux-limited (98% at $r < 19.6$, Driver et al. 2022) galaxy sample.

To build the photo- z error models, we divide the joint spec- z – photo- z data into photo- z bins with a width of $\Delta z = 0.02$ for 2MPZ and $\Delta z = 0.04$ for WISC and fit both Gaussian and modified Lorentzian profiles to Δz distributions obtained for the particular bins to infer parameters a , s , σ and μ for every bin. Then we fit a linear function for each parameter in z_{photo} . Results of our calibration are provided in Appendix A, and are shown for modified-Lorentzian and Gaussian models for the 2MPZ and WISC catalogues respectively in Figures A1 and A2. We set $\mu = 0$ for the rest of this paper for both catalogues because the fitted value is small relative to redshift. Then we refit σ with that assumption. The obtained model is shown in Table 3. We apply the attained model to all galaxies in the catalogues. Obtained distributions are truncated at $z = 0$ and rescaled because redshift below zero is not physical. Moreover, the modified Lorentzian equation is only valid if $a > 0.5$ which corresponds to redshift $z_{\text{photo}} < 0.34$ for 2MPZ and $z_{\text{photo}} < 0.424$ for WISC. There

	2MPZ	WISC
σ	$0.052z_{\text{photo}} + 0.008$	$0.085z_{\text{photo}} + 0.019$
a	$-10.1z_{\text{photo}} + 3.9$	$-4.74z_{\text{photo}} + 2.51$
s	$0.031z_{\text{photo}} + 0.01$	$0.043z_{\text{photo}} + 0.021$

Table 1. The obtained relation of parameters σ , a , s and photometric redshift z_{photo} for 2MPZ and WISC catalogues.

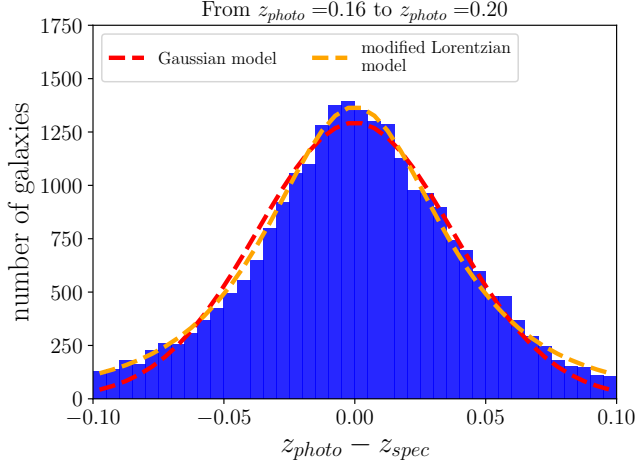


Figure 1. Comparison between Gaussian and modified Lorentzian model of uncertainties. Blue histogram shows the difference between photo- z and spec- z for WISC catalogue for galaxies between $z_{\text{photo}} > 0.28$ and $z_{\text{photo}} < 0.32$. Red (orange) line is a Gaussian (modified Lorentzian) model fitted to the histogram.

are not many galaxies outside of that range so we put a redshift cut there.

This way we have a model for photo- z uncertainty for each galaxy included in a given catalogue. We note however that in the future this approach may need to be more sophisticated, for instance by building different photo- z models for various galaxy populations. For instance, red galaxies are known to have generally better photo- z performance than the blue ones (e.g. Bilicki et al. (2021)) and such details may need to be accounted for as a secondary effects as the statistical error in the H_0 measurement shrinks with an increasing number of GW events.

4 COSMOLOGY INFERENCE

4.1 Methodology and codebase

We employ the pixelated version of the `gwcosmo` code (Gray 2021; Gray et al. 2022) to calculate H_0 from GW data using the galaxy catalogue method. The essential methodology behind the inference is described in Gray et al. (2020); Abbott et al. (2021d). The posterior probability density on H_0 is expressed as a prior $p(H_0)$ times the likelihood from each of the individual events ev , as

$$p(H_0|\{x_{\text{GW}}\}, \{D_{\text{GW}}\}) \propto p(H_0)p(N_{\text{det}}|H_0) \prod_{ev=1}^{N_{\text{det}}} p(x_{\text{GW}}^{\text{ev}}|D_{\text{GW}}^{\text{ev}}, H_0). \quad (2)$$

Here $D_{\text{GW}}^{\text{ev}}$ (subsequently D_{GW}) indicates a positive GW detection and $x_{\text{GW}}^{\text{ev}}$ (subsequently x_{GW}) is the associated GW data. The addi-

tional term $p(N_{\text{det}}|H_0)$ which appears in front of the expression is the probability of detecting N_{det} events; it is marginalized over assuming a uniform in log rate prior $p(R) \propto R^{-1}$, and loses its dependence on H_0 (for more details, see Fishbach et al. 2018; Abbott et al. 2021d).

For each event, the likelihood separates into in-galaxy-catalogue and out-of-galaxy-catalogue parts (denoted respectively by G and \bar{G} below). What is contained in the galaxy catalogue and what is not is governed by the depth of the galaxy survey(s). To the first order, this corresponds to an apparent magnitude threshold m_{th} , which can potentially vary across the sky. The pixelated version of `gwcosmo` allows for such a variation of m_{th} . The sky is first divided into N_{pix} equally-sized pixels following HEALPIX (Górski et al. 2005), and the likelihood is computed by summing over the contributions for each of these pixels i .

$$p(x_{\text{GW}}|D_{\text{GW}}, H_0) = \frac{1}{N_{\text{pix}}} \sum_{i=1}^{N_{\text{pix}}} \left[p_i(x_{\text{GW}}|G, D_{\text{GW}}, H_0)p_i(G|D_{\text{GW}}, H_0) + p_i(x_{\text{GW}}|\bar{G}, D_{\text{GW}}, H_0)p_i(\bar{G}|D_{\text{GW}}, H_0) \right]. \quad (3)$$

Within pixel i , $p_i(G|D_{\text{GW}}, H_0)$ is the probability that the host galaxy is in the catalogue and $p_i(\bar{G}|D_{\text{GW}}, H_0) \equiv 1 - p_i(G|D_{\text{GW}}, H_0)$ the complementary probability that the host galaxy is not in the catalogue.

The in-catalogue likelihood is evaluated as a sum over the redshift distribution of each of the individual galaxies in the catalogue, times the support of the GW likelihood in that sky-direction and distance (given H_0) times the probability of the given galaxy to host or to source the GW event:

$$p_i(x_{\text{GW}}|G, D_{\text{GW}}, s, H_0) = \frac{\sum_{j=1}^{N_{\text{gal}}} \int dz p(x_{\text{GW}}|z, \Omega_j, s, H_0) p(z|z_{\text{photo}}^j) p(s|z) p(s|M(z, m_j, H_0))}{\sum_{j=1}^{N_{\text{gal}}} \int dz p(D_{\text{GW}}|z, \Omega_j, s, H_0) p(z|z_{\text{photo}}^j) p(s|z) p(s|M(z, m_j, H_0))}. \quad (4)$$

The parameter s on the right-hand side of the initial expression is to state the (previously implicit) assumption that there is a real GW source associated with the GW data. Here $p(z_j)$ is the probability distribution of the redshift of the j^{th} galaxy in the catalogue, and Ω_j its sky-direction. The standard `gwcosmo` code assumes a Gaussian for the redshift distribution of the galaxy. We modify the previous code-base so that it is able to include more generic redshift distributions. The second term within the integral above can be obtained from standard GW parameter inference which yields $p(x_{\text{GW}}|d_L, \Omega)$ and using $d_L = d_L(z, H_0)$, with d_L being the luminosity distance. The third term within the integral is the probability of a galaxy at a redshift z to host a GW source $p(s|z)$, evaluated at the galaxy redshift $z = z_j$. This probability is the GW event rate in the source frame $R(z)$ multiplied by the cosmological time dilation factor for conversion from the source frame to the detector frame, $p(s|z) \propto (1+z)^{-1}R(z)$. The final term within the integral, $p(s|M)$, is the probability of a galaxy of absolute magnitude M to host a GW event. This can be used to weight the galaxies in proportion to their luminosities (in a certain observed band),

$$p(s|M(z_j, m_j, H_0)) \propto L(M_j(H_0)). \quad (5)$$

Here m_j is the apparent magnitude of the galaxy z_j and $M_j(H_0) \equiv$

$M(z_j, m_j, H_0)$ is given by the standard expression

$$M_j(H_0) = m_j - 5 \log_{10} \left(\frac{d_L(z_j, H_0)}{\text{Mpc}} \right) - 25. \quad (6)$$

The denominator outside the overall expression is the GW selection function or the *detection efficiency* (Abbott et al. 2017; Mandel et al. 2019) which quantifies the probability of a GW detection (given H_0), and is obtained formally by integrating over all detectable GW data sets $\{x_{\text{GW}}\}$:

$$p_i(D_{\text{GW}}|G, s, H_0) = \int dx_{\text{GW}} p_i(x_{\text{GW}}|G, s, H_0). \quad (7)$$

In practice, the computation of a selection function involves assuming priors on the source distribution (including mass and redshift distributions) and integrating over the cases where the GW event is above a certain signal-to-noise ratio (SNR) threshold and can be assumed to be *detected*.

The out-of-catalogue likelihood is evaluated as an integral instead of a sum over discrete galaxy redshifts, assuming a redshift and sky distribution of the unobserved galaxies and a magnitude distribution of their luminosities, in proportion to their probability of hosting a GW source:

$$p_i(x_{\text{GW}}|\bar{G}, D_{\text{GW}}, s, H_0) = \frac{\int dz d\Omega dM p(x_{\text{GW}}|z, \Omega, s, H_0) p(z) p(\Omega) p(M|H_0) p(s|z) p(s|M)}{\int dz d\Omega dM p(D_{\text{GW}}|z, \Omega, s, H_0) p(z) p(\Omega) p(M|H_0) p(s|z) p(s|M)}. \quad (8)$$

The prior on the redshift is taken to be proportional to the differential comoving volume, $p(z) \propto dV_c(z)/dz$. The sky location prior $p(\Omega)$ is taken to be uniform in the sky. The prior on the absolute magnitude of the galaxies is chosen to be a Schechter function

$$p(M|H_0) \propto 10^{-0.4(\alpha+1)(M-M^*(H_0))} \exp \left[-10^{-0.4(M-M^*(H_0))} \right], \quad (9)$$

described by a characteristic magnitude M^* and a slope α for the given observation band. The remaining terms are obtained as above.

Once again, the denominator obtained by integrating over all the “gravitationally” detectable datasets,

$$p_i(D_{\text{GW}}|\bar{G}, s, H_0) = \int dx_{\text{GW}} p_i(x_{\text{GW}}|\bar{G}, s, H_0). \quad (10)$$

To complete the discussion of the methodology, the in-catalogue probability for each of the pixels is obtained using

$$p_i(G|D_{\text{GW}}, s, H_0) = \frac{\iiint_0^{z(m_{\text{th}}, M, H_0)} dz d\Omega dM I(z, \Omega, M)}{\iiint_0^{\infty} dz d\Omega dM I(z, \Omega, M)}, \quad \text{with} \\ I(z, \Omega, M) \equiv p(D_{\text{GW}}|z, \Omega, M, H_0) p(z) p(\Omega) p(M|H_0) p(s|z) p(s|M). \quad (11)$$

4.2 Data and parameter settings

We stick to the settings of Abbott et al. (2021b) wherever possible. In particular, we choose the same set of GW events with a signal-to-noise ratio (SNR) > 11 . However, since we are interested in redshift uncertainties coming from galaxy catalogues, we consider only the “dark” standard sirens; in particular, we do not include GW170817 in our analysis. As a result, we have 46 events: 42 binary black holes, together with the asymmetric mass binary GW190814, neutron star black hole binaries GW200105 and GW200115, and binary neutron star GW190425.

For each of these events, we use the GW selection function as in Abbott et al. (2021b). The computation of a selection function requires an assumption on the mass distribution of the binaries, their rate evolution, and the sensitivity of the detector network. For the mass distribution we use a power law + peak model Abbott et al. (2021c) with the power law slope of the primary mass distribution $\alpha = 3.78$, the power law slope of the secondary mass distribution $\beta = 0.81$, the primary mass in the mass range $m_{\text{max}} = 112.5M_{\odot}$, $m_{\text{min}} = 4.98M_{\odot}$, with a window scale at the lower mass end $\delta_m = 4.8M_{\odot}$, mean of the Gaussian peak $\mu_g = 32.27M_{\odot}$, standard deviation of the Gaussian peak $\sigma_g = 3.88M_{\odot}$ and the relative weight of the Gaussian peak with respect to the power law quantified by the parameter $\lambda_g = 0.03$. For the rate evolution, we use a Madau-Dickinson model (Madau & Dickinson 2014) with a low-redshift power-law slope $\gamma = 4.59$, a high-redshift power-law slope $k = 2.86$ and a peak at $z_p = 2.47$ separating the two regimes. These are the median values for the joint population-cosmology analysis (without galaxy catalogues) performed in Abbott et al. (2021b) using `icarogw` Mastrogiovanni et al. (2021). We further use the sensitivities from the O1, O2, and O3 observing runs of LIGO and Virgo. The same source-frame prior distributions are also used to reweight the GW posterior samples for each of the 46 events considered.

It is worth noting that changing the mass distribution and the rate evolution parameters from their central values can lead to significant differences in the final result. This was studied in Abbott et al. (2021b), and the results were reported in Figure 11 there. In the meantime, approaches have been developed to *marginalize over* a distribution of these parameters while simultaneously estimating H_0 (Mastrogiovanni et al. 2023b,a; Gray et al. 2023). The assumption of fixed values of mass and rate parameters for an H_0 inference will thus no longer be necessary.

We make a different choice for the galaxy catalogue however, namely, we use 2MPZ and WISC instead of GLADE+. We use the B_J band with Schechter function parameters $M^* = -19.66$ and $\alpha = -1.21$ from Norberg et al. (2002) for both catalogues.

In the first set of runs, we use the standard `gwcosmo` code with Gaussian uncertainties. In the next set of runs, we change the redshift uncertainty profile from a Gaussian to the modified Lorentzian, the rest of the setup being the same as previously. For the third set of runs, we turn off the uncertainties on the redshift altogether. Finally, we artificially alter the redshift uncertainties. For Gaussian uncertainties, this corresponds to multiplying the standard deviation σ by a constant. For the modified Lorentzian case boosting the uncertainties is not straightforward, as the parameters a and s are related, and moreover, the model is only valid if $a > 0.5$, so we artificially shrink the uncertainties by using $a(\frac{1}{2}z_{\text{photo}})$ and $s(\frac{1}{2}z_{\text{photo}})$, for every galaxy with redshift z_{photo} .

5 RESULTS AND DISCUSSION

In this Section we present the result of applying the photo- z error models described in Sec. 3 to the H_0 derivation framework detailed in Sec. 4, based on the 2MPZ and WISC galaxy catalogs. We start however by discussing how the redshifts of different quality influence the observed distribution of galaxies. For that, we generate a mock catalog of uniformly distributed galaxies in the flat Λ CDM background cosmology with $H_0 = 70 \text{ km s}^{-1} \text{ Mpc}^{-1}$ and $\Omega_m = 0.3$. We assume that galaxies follow a Schechter (1976) luminosity function with same parameters as mentioned in Sec. 4.2. Then we assume that the catalogue is magnitude limited with a threshold $m_{\text{obs}}^{B_J} = 21$ mag. This gives us the ‘true’ redshift distribution, shown with the

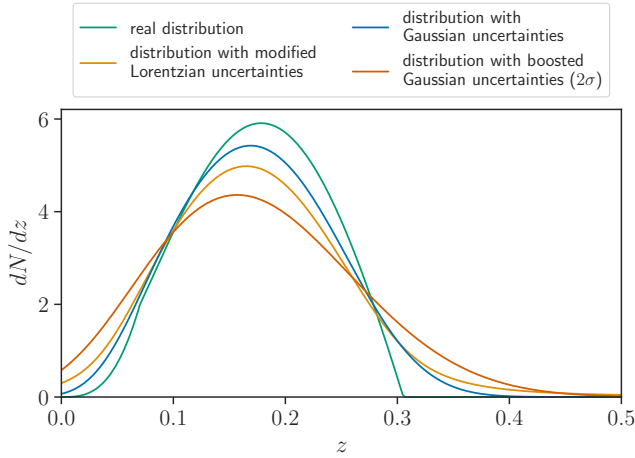


Figure 2. The distribution of observed redshifts in a mock catalogue mimicking the WISC magnitude limit of $m_{B_J} = 21$ mag. We use a background cosmology and model the luminosity distribution of the galaxies as a Schechter function with parameters discussed in the text, and generate the ‘true’ redshift distribution shown with the green line. Then we perturb it with Gaussian (blue line) and modified Lorentzian (yellow line) uncertainties as in the real WISC catalog.

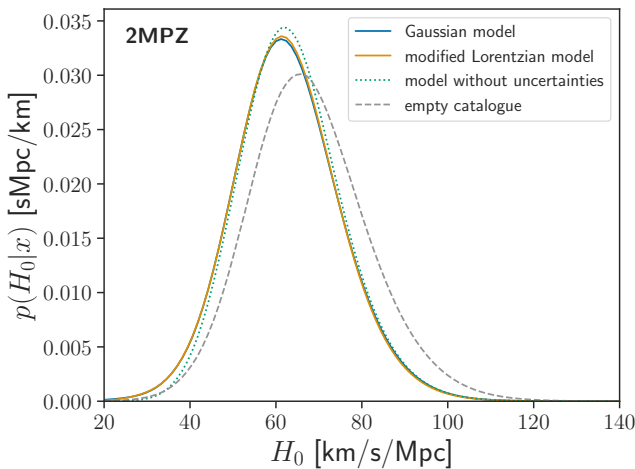


Figure 3. The influence of different redshift uncertainty models on the inference of the Hubble constant based on the 2MPZ catalog. We plot the posterior probability distribution in H_0 obtained using the 46 events used in [Abbott et al. \(2021b\)](#). Results with the Gaussian and modified Lorentzian uncertainty models are plotted in blue and orange, respectively. For reference, we also show the result without any uncertainty on the redshift (dotted green line). As well as an empty catalogue case (dashed gray line).

green line in Fig. 2. Then we perturb these ‘true’ redshifts using the Gaussian and modified Lorentzian redshift uncertainties as calculated in Sec. 3 for the WISC catalog. Applying the uncertainties to a catalogue shifts the whole redshift distribution, as well as its peak, to lower values, and also adds a tail at high redshifts. This shift may influence the statistical derivation of H_0 along with other analysis in which redshift statistics are involved.

To study the influence of the photo- z error models on the H_0 posterior we start by the shallower 2MPZ catalog. Although it covers

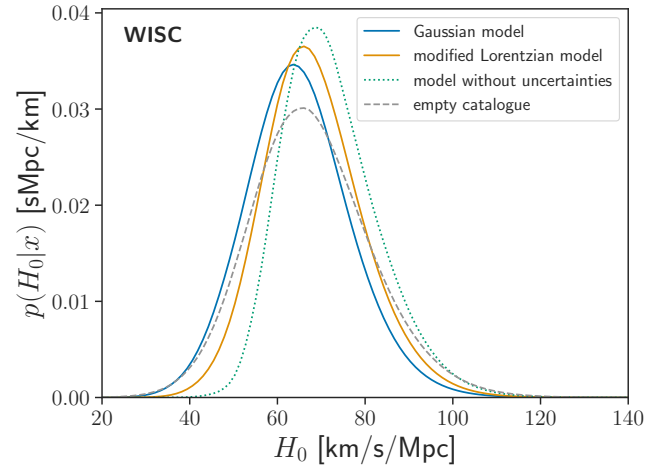


Figure 4. The influence of different redshift uncertainty models on the inference of the Hubble constant based on the WISC catalog. We plot the posterior probability distribution in H_0 obtained using the 46 events used in [Abbott et al. \(2021b\)](#). Results with the Gaussian and modified Lorentzian uncertainty models are plotted in blue and orange respectively. For reference, we also show the result without any uncertainty on the redshift (dotted green line), as well as for the empty catalogue case (dashed grey).

almost the entire sky, and has better-quality redshifts than WISC, it is very shallow when compared to the typical distances of GW events detected by LVK. Only 19 events out of 46 we use from GWTC-3 have estimated distances within 2MPZ coverage of $z < 0.25$ ($d_L \approx 1$ Gpc). Therefore, H_0 derivations using this catalog will be dominated by the out-of-catalog terms and in particular the population model. Indeed, as shown in Fig. 3, the impact of various photo- z models is minimal on the H_0 posterior in that case. The modified Lorentzian and Gaussian case give practically the same results, and the idealized case of no uncertainties is only slightly different. This latter is not representing the actual situation, as it assumes that the redshifts reported in the 2MPZ catalog are exact. We show it just for comparison as an ‘upper limit’, equivalent to the hypothetical case of spectroscopic redshifts with negligible uncertainties. We also add the empty catalogue case: a ‘lower limit’, with a redshift prior coming only from the background cosmology, and with no information from galaxies. The main results of this comparison is that catalogs of such a depth as 2MPZ do not provide enough information to significantly change the posterior with that method, therefore we do not further analyse this case.

We now turn to the comparison of different redshift uncertainty models for the WISC catalogue, shown in Figure 4. Moreover we add already discussed upper-limit case of no redshift uncertainties and lower-limit of empty catalogue. Introducing Gaussian or modified Lorentzian uncertainty models moves the peak of the distribution to support lower values of H_0 . This can be understood by recalling Figure 2. Introducing the uncertainty to the galaxy catalogue impacts the distribution of the observed redshifts. As detailed in Sec. 3, the uncertainties of our models grow with redshift, therefore low-redshift galaxies are less impacted by the scatter. However the change in uncertainty is significant at the peak of the redshift distribution by scattering galaxies from that area to lower and higher redshifts. Galaxies from the high end of the redshift range have large uncertainties, thus they can be scattered into very high redshifts causing the tail of the distribution to appear. All that causes the peak of

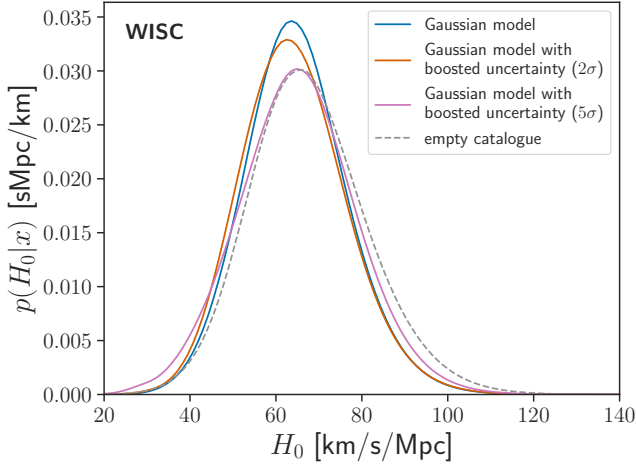


Figure 5. The influence of boosting the redshift uncertainty in the Gaussian model for the WISC catalogue. We plot the H_0 posterior density with the Gaussian model as fitted to date (blue), with the Gaussian model but uncertainties enhanced by a factor of 2 (orange), and one with the uncertainties enhanced by a factor of 5 (pink).

the distribution to move to lower redshift values and thus supporting lower values of H_0 . Moreover, there is an additional effect for the modified Lorentzian case. The truncation of the redshift posterior of each galaxy at $z = 0$ causes the mean of the posterior to move to higher values, which correspond to supporting higher values of H_0 . This truncation is significant for modified Lorentzian distribution but not for Gaussian distribution. That is the reason why the modified Lorentzian model peak of H_0 is to the right of the Gaussian model peak.

The influence of artificially boosting redshift uncertainties for the Gaussian model is shown in Figure 5. When increasing the scatter σ , not only does the posterior of H_0 widen, but also the peak of the distribution shifts. For the 2σ case the peak moves to the left, because the distribution of observed redshifts shifts to lower values as the uncertainties increase, as shown in Figure 2. However, for the 5σ case the distribution moves to the right, and overlaps with the empty catalogue case. This is because for such large uncertainties (amounting to between 0.1 up to 0.25) the catalogue is uninformative and the posterior of H_0 is dominated by the out-of-catalogue part, and is pushed towards the empty catalogue case.

The last case we studied was to artificially change the modified Lorentzian uncertainties. This is not as straightforward as for the Gaussian, because the model given by Eq. (1) puts a limit on the parameter $a > 0.5$. Therefore, the best-fit model for WISC is valid only when $z_{\text{photo}} < 0.424$. Moreover, the parameters s and a are not independent and both are responsible for the shape of the distribution. Hence, to preserve the realistic shape of the error distribution, instead of varying a and s directly, we modify the model by using for a galaxy with z_{photo} , the redshift error value that would be assigned to an object with $0.5 * z_{\text{photo}}$, effectively choosing the error of twice as small redshift. The result is shown in Figure 6. Decreasing the uncertainty this way has a minimal effect on the shape of the H_0 posterior.

To conclude this section, we study the above effects focusing on a single GW detection, GW190814, and the WISC catalogue. GW190814 is the best-localized dark standard siren to date, and it was seen in Abbott et al. (2021b) that it is one of the few events in GWTC-3

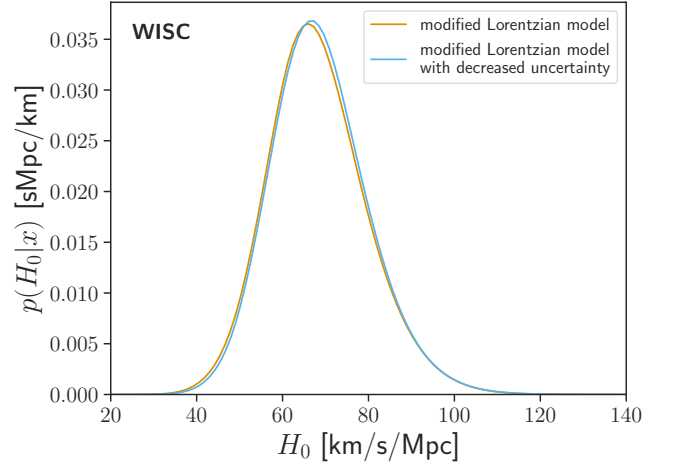


Figure 6. The influence of decreasing the redshift uncertainty in the modified Lorentzian model for the WISC catalogue. We plot the H_0 posterior density with the best-fit modified Lorentzian model (blue), and the same model but with uncertainties taken for galaxies at twice smaller redshift (orange; see details in the text). This change does not have a significant impact on the H_0 posterior.

with significant in-catalogue information. The posterior distributions on H_0 with Gaussian, modified-Lorentzian, and without redshift uncertainties are shown in Figure 7. In this case, we see a significant difference with and without redshift uncertainties and also a more visible difference coming from different uncertainty profiles. Turning off the redshift uncertainties altogether leads to H_0 peaking at higher values. This is explained by an overdensity of galaxies along the line of sight of GW190814 seen at a redshift of around 0.22 when redshift uncertainties are not considered. We discuss this further in Appendix B. Since this overdensity vanishes when redshift uncertainties are included, it is not a real feature in the data. These results further highlight the importance of including proper redshift uncertainties in a dark standard siren measurement of H_0 .

6 CONCLUSIONS AND OUTLOOK

In this paper, we looked into the impact of redshift uncertainties of potential host galaxies on a dark GW standard-siren measurement of H_0 . We first constructed Gaussian and modified Lorentzian uncertainty models for two catalogues: WISC and 2MPZ. Then we modified the *gwcosmo* code to handle the modified Lorentzian uncertainty model. We used the same set of 46 gravitational sources as in Abbott et al. (2021b) to obtain the H_0 posterior with WISC and 2MPZ catalogues and with Gaussian, modified Lorentzian, and no uncertainty models of redshift uncertainties. Redshift uncertainties have an impact on the observed redshift distribution of galaxies in a catalogue and thus have an impact on the statistical inference of H_0 . The impact is particularly large in the case of well-localized GW events with significant in-catalogue contributions such as GW190814. The impact however is not statistically significant with the current ensemble of GW detections. It is worth highlighting that the impact on H_0 of different redshift uncertainty profiles (as seen in Figure 4, for example) is slightly smaller, but of the same order of magnitude as some of the principal sources of systematic errors in Abbott et al. (2021b), namely the uncertainty in compact binary population model

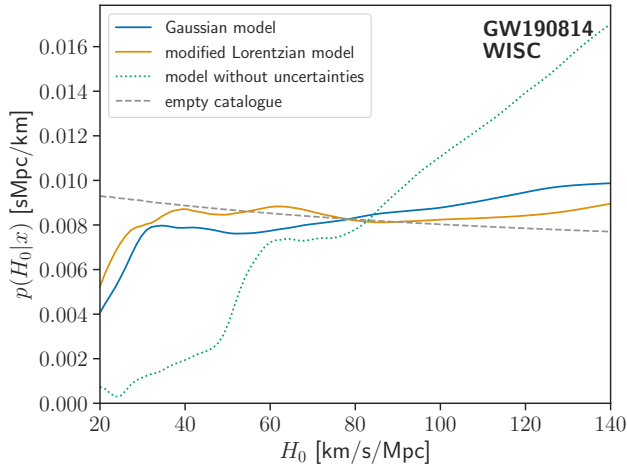


Figure 7. The influence of redshift uncertainties on the H_0 obtained from the single well-localized event GW190814 which has a significant in-galaxy-catalog contribution. In this case, we see a visible difference between the result with Gaussian and modified-Lorentzian uncertainties and a significant change when redshift uncertainties are turned off altogether. We would like to emphasise that the result obtained without redshift uncertainties is not to be trusted due to reasons explained in the text.

parameters (Figure 11 of Abbott et al. 2021b). It is to be noted that while this work was in preparation, two separate methods, Mastrogiovanni et al. (2023b,a) and Gray et al. (2023), were developed for marginalizing over the unknown parameters of the population model, potentially making uncertainties coming from the galaxy catalogue sector the leading source of possible systematic errors in the dark standard siren H_0 measurement.

The relative importance of redshift uncertainties is expected to increase in the course of the future observing runs as more GW events come in and the statistical measurement errors are reduced. Moreover, uncertainties coming from the galaxy catalogue sector are expected to become more important with future deeper galaxy surveys. We recommend a follow-up mock data challenge in order to investigate various sources of systematic uncertainties important for the fourth observing run of the LVK detector network. Along with other objectives, we expect this mock data challenge to also tell us the exact conditions when redshift uncertainty models will become significantly important.

ACKNOWLEDGEMENTS

We would like to thank Tessa Baker, Freija Beirnaert, Martin Hendry, Christos Karathanasis, Simone Mastrogiovanni, Surhud More, Sudip Mukherjee, Federico Stachurski, and Nicola Tamanini for fruitful discussions throughout the project, and additionally Stefano Rinaldi and Aditya Vijaykumar for useful comments on the manuscript. We would also like to thank the anonymous referee for suggesting additional analysis which strengthened our conclusions.

The research of CT, GD, and AG is supported by the Ghent University Special Research Funds (BOF) project BOF/STA/202009/040 and the Fonds Wetenschappelijk Onderzoek (FWO) iBOF project BOF20/IBF/124. The research of RG is supported by the European Research Council, starting grant SHADE 949572. MB is supported by the Polish National Science Center

through grants no. 2020/38/E/ST9/00395, 2018/30/E/ST9/00698, 2018/31/G/ST9/03388 and 2020/39/B/ST9/03494, and by the Polish Ministry of Science and Higher Education through grant DIR/WK/2018/12.

This material is based upon work supported by NSF’s LIGO Laboratory which is a major facility fully funded by the National Science Foundation. The computing runs for the cosmology inference using `gwcosmo` have been performed on the LIGO Data Grid computer clusters. The authors are grateful for computational resources provided by the LIGO Laboratory and supported by National Science Foundation Grants PHY-0757058 and PHY-0823459. This work makes use of `gwcosmo` which is available at <https://git.ligo.org/lscsoft/gwcosmo>.

This manuscript was reviewed by the LIGO Scientific Collaboration (document number: LIGO-P2300044) and by the Virgo Collaboration (document number: VIR-0147A-23).

DATA AVAILABILITY

The 2MPZ and the WISC catalogues are available at <http://ssa.roe.ac.uk/TWOMPZ.html>, and at <http://ssa.roe.ac.uk/WISEXSCOS.html>, respectively. All of the GW events we have used in this analysis are available at <https://www.gw-openscience.org/>.

APPENDIX A: REDSHIFT UNCERTAINTY MODEL CALIBRATION

As we do not have individual photo- z PDFs nor photo- z uncertainties for each photometric galaxy, we use a calibration spectroscopic sample to build a photo- z error model for the entire photometric sample. To go beyond the 0th order approximation where this model would be the same for all the galaxies (i.e. independent of any observable quantity), we assume that the shape of the photo- z PDF will depend on the photo- z itself (it could instead, or also, depend for instance on galaxy magnitude or color). We could then fit a linear (or any other) relation between the photo- z and its mean error based on the individual $z_{\text{phot}} - z_{\text{spec}}$ residuals. However, we want to model also the scatter (standard deviation in the Gaussian case, or more generally the wings of the modified Lorentzian distribution), which requires some binning. For good statistics we choose relatively broad bins in photo- z and the parameters of the model are derived for these bins, but still as simple functions of photo- z . This allows us to build generalised models as a function of redshift.

We consider Gaussian and modified-Lorentzian uncertainty models with parameters described in the main text in Section 3. We assume linear dependence of each parameter and photometric redshift then we fit linear function for 2MPZ and WISC. Results are shown in Figure A1 and A2 respectively.

APPENDIX B: GALAXY OVERDENSITIES ALONG THE LINE-OF-SIGHT OF GW190814

In order to investigate the behaviour seen in Figure 7, we look at the redshift distribution of galaxies in the WISC catalogue along the line-of-sight of GW190814 with different uncertainty models. We find an overdensity around $z = 0.24$ when redshift uncertainties are turned off, which is extraneous and goes away as soon as these uncertainties are taken into account. This explains why H_0 tend to favour higher values in the absence of redshift uncertainties in Figure 7.

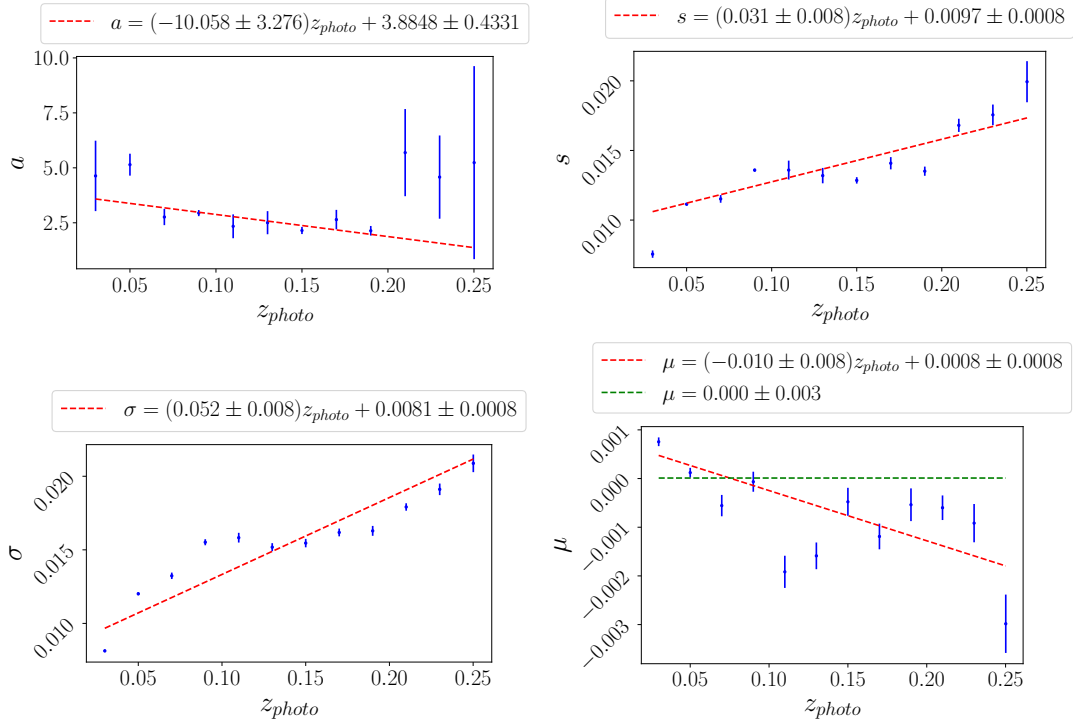


Figure A1. Models of parameters a , s for modified Lorentzian model (top) and σ , μ for Gaussian model (bottom) obtained for 2MPZ from the calibration sample. Points represent parameters obtained from each bin and the middle of each bin. We use $\mu = 0$ for our further calculations.

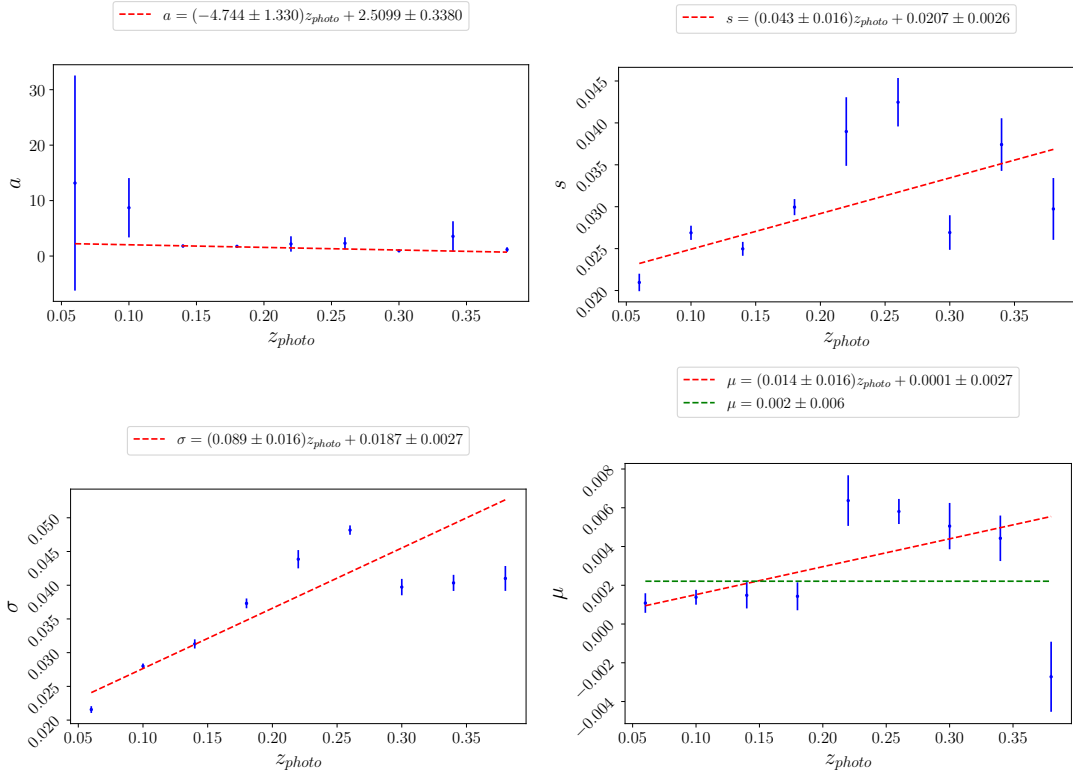


Figure A2. Models of parameters a , s for modified Lorentzian model (top) and σ , μ for Gaussian model (bottom) obtained for WISC from the calibration sample. Points represent parameters obtained from each bin and the middle of each bin. We use $\mu = 0$ for our further calculations.

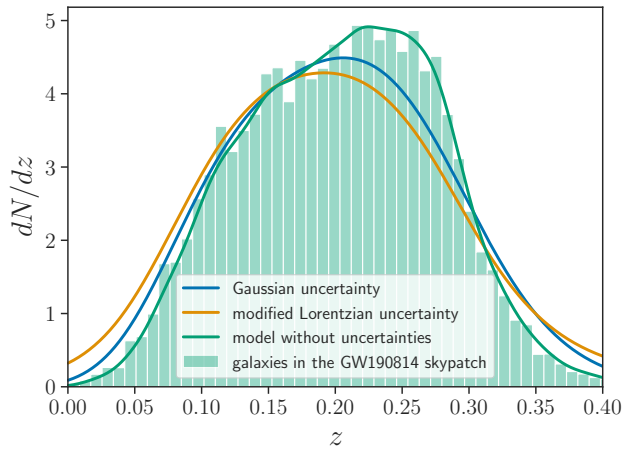


Figure B1. The redshift distribution from galaxies from the WISC catalogue along the line-of-sight of GW190814. The 90% sky area is considered. As in the rest of the manuscript, we consider the Gaussian and Lorentzian redshift uncertainty models, and also no redshift uncertainties. In the absence of redshift uncertainties, we see an overdensity of galaxies around $z = 0.24$, which goes away when uncertainties are taken into account.

REFERENCES

- Abbott B. P., Abbott R., Abbott T. D., et al., 2016, *Phys. Rev. Lett.*, **116**, 061102
- Abbott B. P., et al., 2017, *Nature*, **551**, 85
- Abbott R., et al., 2020, *Astrophys. J. Lett.*, **896**, L44
- Abbott R., et al., 2021b
- Abbott R., et al., 2021a
- Abbott R., et al., 2021c
- Abbott B. P., et al., 2021d, *Astrophys. J.*, **909**, 218
- Aghanim N., et al., 2020, *Astron. Astrophys.*, **641**, A6
- Ahn C. P., Alexandroff R., Allende Prieto C., et al., 2012, *ApJS*, **203**, 21
- Alam S., Albareti F. D., Allende Prieto C., et al., 2015, *ApJS*, **219**, 12
- Balaguera-Antolínez A., Bilicki M., Branchini E., Postiglione A., 2018, *MNRAS*, **476**, 1050
- Bilicki M., Jarrett T. H., Peacock J. A., Cluver M. E., Steward L., 2014, *ApJS*, **210**, 9
- Bilicki M., Peacock J. A., Jarrett T. H., et al., 2016, *ApJS*, **225**, 5
- Bilicki M., et al., 2021, *A&A*, **653**, A82
- Chambers K. C., Magnier E. A., Metcalfe N., et al., 2016, *arXiv e-prints*, p. [arXiv:1612.05560](https://arxiv.org/abs/1612.05560)
- Chen H.-Y., Fishbach M., Holz D. E., 2018, *Nature*, **562**, 545
- Colless M., Dalton G., Maddox S., et al., 2001, *MNRAS*, **328**, 1039
- Collister A. A., Lahav O., 2004, *PASP*, **116**, 345
- Cutri R. M., et al., 2012, *VizieR Online Data Catalog*, p. [II/311](https://vizier.cesr.cnr.it/cgi-bin/request/all?source=VizieR%20Online%20Data%20Catalog&sourceID=II/311)
- Cutri R. M., Wright E. L., Conrow T., et al., 2021, *VizieR Online Data Catalog*, p. [II/328](https://vizier.cesr.cnr.it/cgi-bin/request/all?source=VizieR%20Online%20Data%20Catalog&sourceID=II/328)
- DESI Collaboration et al., 2016, *arXiv e-prints*, p. [arXiv:1611.00036](https://arxiv.org/abs/1611.00036)
- Dainotti M. G., De Simone B., Schiavone T., Montani G., Rinaldi E., Lambiase G., 2021, *ApJ*, **912**, 150
- Dainotti M. G., De Simone B. D., Schiavone T., Montani G., Rinaldi E., Lambiase G., Bogdan M., Ugale S., 2022, *Galaxies*, **10**, 24
- Dálya G., Galgóczi G., Dobos L., et al., 2018, *MNRAS*, **479**, 2374
- Dálya G., Díaz R., Bouchet F. R., et al., 2022, *MNRAS*, **514**, 1403
- Del Pozzo W., 2012, *Phys. Rev. D*, **86**, 043011
- Dey A., Schlegel D. J., Lang D., et al., 2019, *AJ*, **157**, 168
- Driver S. P., Norberg P., Baldry I. K., et al., 2009, *Astronomy and Geophysics*, **50**, 5.12
- Driver S. P., Bellstedt S., Robotham A. S. G., et al., 2022, *MNRAS*, **513**, 439
- Farr W. M., Fishbach M., Ye J., Holz D., 2019, *Astrophys. J. Lett.*, **883**, L42
- Finke A., Foffa S., Iacovelli F., Maggiore M., Mancarella M., 2021, *JCAP*, **08**, 026
- Fishbach M., Holz D. E., Farr W. M., 2018, *Astrophys. J. Lett.*, **863**, L41
- Fishbach M., et al., 2019a, *Astrophys. J. Lett.*, **871**, L13
- Fishbach M., et al., 2019b, *Astrophys. J. Lett.*, **871**, L13
- Górski K. M., Hivon E., Banday A. J., Wandelt B. D., Hansen F. K., Reinecke M., Bartelman M., 2005, *Astrophys. J.*, **622**, 759
- Gray R., 2021, PhD thesis, University of Glasgow, [doi:10.5525/gla.thesis.82438](https://doi.org/10.5525/gla.thesis.82438)
- Gray R., et al., 2020, *Phys. Rev. D*, **101**, 122001
- Gray R., Messenger C., Veitch J., 2022, *Mon. Not. Roy. Astron. Soc.*, **512**, 1127
- Gray R., et al., 2023
- Hambly N. C., MacGillivray H. T., Read M. A., et al., 2001, *MNRAS*, **326**, 1279
- Hang Q., Alam S., Peacock J. A., Cai Y.-C., 2021, *MNRAS*, **501**, 1481
- Holz D. E., Hughes S. A., 2005, *Astrophys. J.*, **629**, 15
- Howlett C., Davis T. M., 2020, *Monthly Notices of the Royal Astronomical Society*, **492**, 3803
- Huchra J. P., Macri L. M., Masters K. L., et al., 2012, *ApJS*, **199**, 26
- Jarrett T. H., Chester T., Cutri R., et al., 2000, *AJ*, **119**, 2498
- Jones D. H., Read M. A., Saunders W., et al., 2009, *MNRAS*, **399**, 683
- Laureijs R., et al., 2011, *arXiv e-prints*, p. [arXiv:1110.3193](https://arxiv.org/abs/1110.3193)
- Liske J., Baldry I. K., Driver S. P., et al., 2015, *MNRAS*, **452**, 2087
- Lyke B. W., Higley A. N., McLane J. N., et al., 2020, *ApJS*, **250**, 8
- MacLeod C. L., Hogan C. J., 2008, *Phys. Rev. D*, **77**, 043512
- Madau P., Dickinson M., 2014, *Ann. Rev. Astron. Astrophys.*, **52**, 415
- Makarov D., Prugniel P., Terekhova N., Courtois H., Vauglin I., 2014, *A&A*, **570**, A13
- Mandel I., Farr W. M., Gair J. R., 2019, *Mon. Not. Roy. Astron. Soc.*, **486**, 1086
- Mastrogiovanni S., et al., 2021, *Phys. Rev. D*, **104**, 062009
- Mastrogiovanni S., et al., 2023a
- Mastrogiovanni S., et al., 2023b, *Phys. Rev. D*, **108**, 042002
- Mukherjee S., Lavaux G., Bouchet F. R., Jasche J., Wandelt B. D., Nissanke S., Leclercq F., Hotokezaka K., 2021, *A&A*, **646**, A65
- Nicolaou C., Lahav O., Lemos P., Hartley W., Braden J., 2020, *Monthly Notices of the Royal Astronomical Society*, **495**, 90
- Nissanke S., Holz D. E., Hughes S. A., Dalal N., Sievers J. L., 2010, *Astrophys. J.*, **725**, 496
- Norberg P., Cole S., Baugh C. M., et al., 2002, *MNRAS*, **336**, 907
- Palmese A., et al., 2020, *Astrophys. J. Lett.*, **900**, L33
- Palmese A., Bom C. R., Mucesh S., Hartley W. G., 2023, *The Astrophysical Journal*, **943**, 56
- Peacock J. A., Bilicki M., 2018, *MNRAS*, **481**, 1133
- Peacock J. A., Hambly N. C., Bilicki M., et al., 2016, *MNRAS*, **462**, 2085
- Riess A. G., et al., 2022, *ApJ*, **934**, L7
- Schechter P., 1976, *ApJ*, **203**, 297
- Schutz B. F., 1986, *Nature*, **323**, 310
- Skrutskie M. F., Cutri R. M., Stiening R., et al., 2006, *AJ*, **131**, 1163
- Soares-Santos M., et al., 2019, *Astrophys. J. Lett.*, **876**, L7
- Taylor S. R., Gair J. R., Mandel I., 2012, *Phys. Rev. D*, **85**, 023535
- Vakili M., et al., 2020, *arXiv e-prints*, p. [arXiv:2008.13154](https://arxiv.org/abs/2008.13154)
- White D. J., Daw E. J., Dhillon V. S., 2011, *Classical and Quantum Gravity*, **28**, 085016
- Wright E. L., Eisenhardt P. R. M., Mainzer A. K., et al., 2010, *AJ*, **140**, 1868
- de Jong R. S., et al., 2019, *The Messenger*, **175**, 3

This paper has been typeset from a $\text{\TeX}/\text{\LaTeX}$ file prepared by the author.